Resonance Raman Spectroscopy Reveals pH-Dependent Active Site Structural Changes of Lactoperoxidase Compound 0 and Its Ferryl Heme O–O Bond Cleavage Products

ARTICLE *in* JOURNAL OF THE AMERICAN CHEMICAL SOCIETY · DECEMBER 2014

Impact Factor: 12.11 · DOI: 10.1021/ja5107833 · Source: PubMed

4 AUTHORS, INCLUDING:

Piotr Mak

Marquette University

24 PUBLICATIONS **241** CITATIONS

SEE PROFILE

JACS
JOURNAL OF THE AMERICAN CHEMICAL SOCIETY
Article
pubs.acs.org/JACS

Resonance Raman Spectroscopy Reveals pH-Dependent Active Site Structural Changes of Lactoperoxidase Compound 0 and Its Ferryl Heme O−O Bond Cleavage Products

Piotr J. Mak, Warut Thammawichai, Dennis Wiedenhoeft, and James R. Kincaid*

Department of Chemistry, Marquette University, Milwaukee, Wisconsin 53233, United States

Supporting Information

ABSTRACT: The first step in the enzymatic cycle of mammalian peroxidases, including lactoperoxidase (LPO), is binding of hydrogen peroxide to the ferric resting state to form a ferric-hydroperoxo intermediate designated as Compound 0, the residual proton temporarily associating with the distal pocket His109 residue. Upon delivery of this "stored" proton to the hydroperoxo fragment, it rapidly undergoes O−O bond cleavage, thereby thwarting efforts to trap it using rapid mixing methods. Fortunately, as shown herein, both the peroxo and the hydroperoxo (Compound 0) forms of LPO can be trapped by cryoradiolysis, with acquisition of their resonance Raman (rR) spectra now permitting structural characterization of their key Fe−O−O fragments. Studies were conducted under both acidic and alkaline conditions, revealing pH-dependent differences in relative populations of these intermediates. Furthermore, upon annealing, the low pH samples convert to two forms of a ferryl heme O−O bond-cleavage product, whose ν(Fe═O) frequencies reflect substantially different Fe═O bond strengths. In the process of conducting these studies, rR structural characterization of the dioxygen adduct of LPO, commonly called Compound III, has also been completed, demonstrating a substantial difference in the strengths of the Fe−O linkage of the Fe−O−O fragment under acidic and alkaline conditions, an effect most reasonably attributed to a corresponding weakening of the trans-axial histidyl imidazole linkage at lower pH. Collectively, these new results provide important insight into the impact of pH on the disposition of the key Fe−O−O and Fe═O fragments of intermediates that arise in the enzymatic cycles of LPO, other mammalian peroxidases, and related proteins.

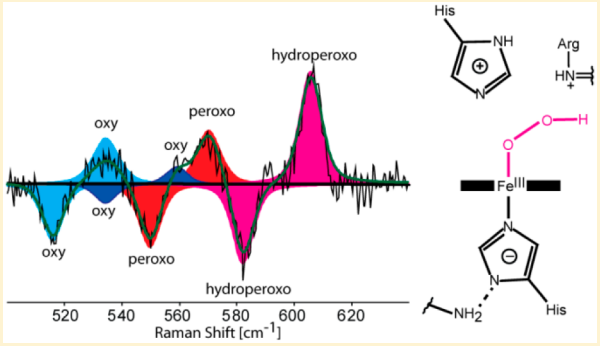

INTRODUCTION

Lactoperoxidase (LPO), a secretory glycohemoprotein that belongs to the mammalian peroxidase superfamily, plays an important role in the innate immune defense system by generating the antimicrobial hypothiocyanate ion via oxidation of thiocyanate, employing endogenous hydrogen peroxide as the primary oxidant.[1,2] Similar to other mammalian peroxidases and some other heme proteins, including cytochrome c,[3] the heme group in this enzyme is covalently linked to the protein matrix. Recent crystallographic data of buffalo and bovine LPOs,[4,5] as well as previous magnetic circular dichroism[6] and NMR studies,[7] show that the prosthetic group of LPO is a modified derivative of protoheme, known as heme l, which bears ester linkages formed between two hydroxymethyl groups of heme l at positions 1 and 5 and the protein side chains of glutamate-258 (Glu258) and aspartate-108 (Asp108), respectively (Figure 1).[4−7] These covalent linkages, present in LPO and other mammalian peroxidases, serve to mediate protein-induced strain that results in an unusual degree of out-of-plane distortion of the heme prothetic groups,[4,5] evidence for which had been obtained in earlier spectroscopic studies.[9,10]

The heme iron is coordinated to the imidazole fragment of the proximal histidine (His351) as the fifth ligand. Until recently, it had been accepted that the proximal histidyl imidazole residue of LPO and other mammalian peroxidases

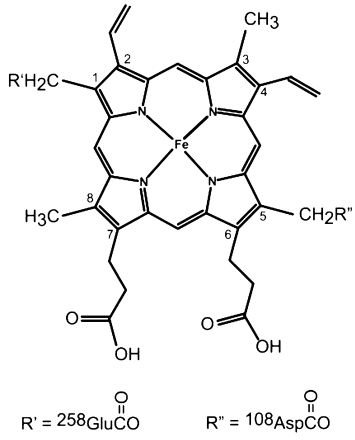

Figure 1. Scheme of heme l in LPO.

Received: October 20, 2014
Published: December 15, 2014

DOI: 10.1021/ja5107833
J. Am. Chem. Soc. 2015, 137, 349−361

are H-bonded to a nearby, strictly conserved, Asn residue postulated to serve as an H-bond acceptor,[11] much as occurs for the plant proximal histidyl imidazoles that interact with a strictly conserved Asp residue, a strong H-bond acceptor.[12,13] However, inasmuch as the Asn of mammalian proxidases is a much weaker H-bond acceptor, it was difficult to rationalize how such a configuration could give rise to the strong iron–nitrogen bonds documented for LPO and MPO, as measured by crystallographic distances and relatively high frequencies for the $\nu(Fe-N_{His})$ stretching modes observed in the resonance Raman spectra.[14] Finally, acquisition of crucial experimental data and thoughtful analysis of related computational results led to a satisfying interpretation that invokes cooperative H-bonding interactions of a proximal side Arg-Asn-His ensemble that requires a heme-coordinated histidyl imidazolate residue, thereby reconciling the substantially elevated $\nu(Fe-N_{His})$ frequencies (Figure 2).[11]

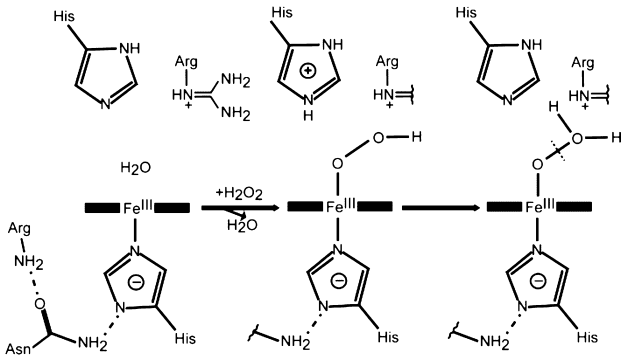

Figure 2. Mechanism of Compound 0 formation in LPO.

The distal side of LPO contains a relatively constrained ligand binding site[4,5,8] and houses additional structural features that play crucial roles in the peroxidase catalytic cycle, including the imidazole of the distal His109 (pK_a 5.8)[15] and Arg255, the former serving as a general acid–base catalyst needed for the required deprotonation step involved in binding of H_2O_2 and the latter mainly acting to stabilize developing negative charge on the terminal oxygen fragment during the O–O bond cleavage process (vide infra) (Figure 2). The first step of the LPO catalytic cycle is binding of hydrogen peroxide to the ferric state to form a fleeting ferric-hydroperoxo intermediate designated as Compound 0, temporarily storing the residual proton at the deprotonated (i.e., nonionized) His109 residue (Figure 2).[16−18] Subsequent delivery of this stored proton to the terminal oxygen of the bound hydroperoxo fragment of LPO Compound 0 triggers rapid heterolytic cleavage of the O–O bond, releasing a water molecule and forming a two-electron oxidized reactive intermediate, with the oxidizing equivalents presumably being initially localized on the heme as a ferryl heme π-cation radical, a species typically referred to as Compound I in the case of plant peroxidases and other oxidative heme enzymes.[1−3,16−18] However, in the case of LPO and other mammalian peroxidases, this Compound I species spontaneously undergoes an internal oxidation–reduction process where the Compound I transient oxidizes an aromatic protein residue, thereby producing a ferryl heme and a protein-based radical, the latter commonly being designated as $aa^{\bullet}$; typically the radical site involves a tyrosine or tryptophan residue.[16−19]

In the case of LPO and other mammalian peroxidases, this overall process occurs with such efficiency that the primary intermediate, Compound 0, has eluded definitive structural characterization until now. The problem arising is that the primary oxidant, H_2O_2, carries with it into the active site the proton that ultimately facilitates the O–O bond cleavage reaction, making it quite difficult, using rapid mixing methods, to effectively isolate Compound 0.[20−22] To trap and structurally characterize this key intermediate, a method is required that can generate it while also preventing delivery of the catalytic ("stored") proton, a seemingly difficult task. However, as is demonstrated in these current studies, the cryoradiolysis approach initiated by Symons and extended by others[23−25] does provide an effective method to generate and trap a hydroperoxo intermediate within the LPO active site in the absence of the catalytic proton. In this way, the peroxo and/or hydroperoxo derivatives of plant and nonmammalian hydroperoxidases,[26,27] as well as those of bacterial and animal cytochromes P450 and related enzymes, have been trapped and characterized by EPR and ENDOR techniques,[28−31] with reports of a crystallographically characterized cryoreduced form of a fungal peroxidase,[32] CYP101,[33] myoglobin,[34] and a few others.[35,36]

In brief, the essential concept involved in cryoradiolysis is to freeze-trap the relatively stable dioxygen adduct, $Fe-O_2$ [formally $Fe(III)-(O-O^{-})$], of heme proteins within an aqueous buffer containing glycerol or certain other organic compounds; in the case of LPO and other peroxidases, this species is designated as Compound III.[16−18,37] Upon irradiation with γ-rays, free-electrons and organic radicals are produced, the electrons being mobile, while other movements, including proton transport, are more restricted.[25] The freeze-trapped $[Fe(III)-(O-O^{2-})]$ peroxo fragment is generated and can be spectroscopically characterized.[28−31] Careful annealing to higher temperatures permits proton transfer that, depending upon the ability of a given protein to transport protons to its active site, can lead to formation and trapping of the hydroperoxo species (Fe(III)–O–O–H), while further annealing can lead to delivery of another proton to facilitate the O–O bond cleavage and product formation, as in the case of CYP101,[28] or possibly to the loss of the bound hydroperoxo fragment, an example of which is documented in the case of the T252A mutant of CYP101.[28] In fact, this cryoradiolysis method, combined with the powerful capability of resonance Raman (rR) spectroscopy, has been recently applied to generate, trap, and structurally characterize the key Fe–O–O and Fe–O–O–H fragments of ferric peroxo and hydroperoxo derivatives of several different proteins, including human globins as well as bacterial cytochromes P450.[38−42]

Inasmuch as mammalian peroxidases play critical roles in human physiology in both normal and diseased states,[43] drawing keen interest from the pharmaceutical industry as potential drug targets,[43] they are naturally attractive, but as yet neglected, candidates for study by the methods described above. Responding to this opportunity, this combination of methods, hereafter referred to as rR/cryoradiolysis, is used here to generate and structurally characterize, for the first time, the peroxo and hydroperoxo derivatives of LPO under varying pH conditions and to document the nature of their O–O bond cleavage ferryl heme products, which are seen to differ between acidic and alkaline pH. In the process, earlier studies of the rR characterization of LPO Compound III, performed at pH 7.0,[44] have been extended to samples buffered at pH 5.6 and 8.2,

DOI: 10.1021/ja5107833
J. Am. Chem. Soc. 2015, 137, 349−361

where it is now revealed that pH-dependent changes in the linkage between the heme iron and the proximal N_{His} donor group are sufficient to account for significant pH-induced alterations in the strength of the Fe−O linkage of LPO Compound III, as directly reflected in substantial shifts of the ν(Fe−O) stretching mode. This combination of newly acquired data for the Compound III, Compound 0, and ferryl heme derivatives of LPO at varying pH values, differing in the protonation status of the key distal histidine residue, as well as differences in the proximal side "push effect" associated with the strength of the Fe−N_{His} linkage,[12,45] provides useful insight into the effect of pH on the disposition of the Fe−O−O and Fe═O fragments of these species and serves to demonstrate the power of this approach for future studies of the active site structures of the catalytic intermediates of mammalian peroxidases in the presence of natural substrates and potential drug candidates.

EXPERIMENTAL METHODS

Isolation and Purification of Lactoperoxidase. Lactoperoxidase (LPO) was isolated from unpasteurized bovine milk obtained from a local dairy farm using Amberlite CG-50 weak cation exchanger resin according to previously published procedures.[46,47] Isolated raw material was further purified by cation exchange chromatography (CM-52), followed by two Bio-Gel P-100 (10 mM phosphate buffer, pH 6.8) column separations to obtain LPO fractions with Rz value (A_{412}/A_{280}) greater than 0.90.[18,48] The final Rz value of the enzyme was 0.92, and approximately 0.420 g of pure LPO was obtained from 60 L of unpasteurized milk. The electronic absorption spectrum (Hewlett-Packard 8452A spectrophotometer) of the LPO resting state exhibits the Soret band at 412 nm and Q-bands at 500, 543, and 590 nm, as well as a ferric-heme charge transfer band at 630 nm, in agreement with the previously published data.[18,48]

Preparation of Lactoperoxidase Intermediates. Ferric LPO samples were prepared by equilibrating the enzyme with 50 mM phosphate or acetate buffers at pH (pD) 8.2 and 5.6, respectively; for example, the pD was adjusted employing pD = pH(meter reading) + 0.4 formula. All samples contained 20% (v/v) purified glycerol or, when needed, glycerol-$(OD)_3$; the glycerol was purified by vacuum distillation. The final concentration of protein was 300 μM with 0.92 Rz value. The heme concentration was calculated according to the millimolar absorptivity at the Soret maximum at 412 nm, 114 mM^{-1} cm^{-1}.[18,48] Ferrous LPO samples were obtained by anaerobic reduction of ferric LPO with approximately 3−4 mol equiv of dithionite solution at room temperature, and the reduction was confirmed by electronic absorption spectrophotometry (the Q-bands of the ferrous form being at 562 and 597 nm).[18] The dithionite solution was prepared anaerobically and was used fresh, and its concentration was determined spectrophotometrically using ε_{316} = 8500 mM^{-1} cm^{-1}.[49] The LPO compound III was prepared in NMR tubes connected to the Schlenck line by sequential application of vacuum, high purity argon, vacuum, and then gaseous oxygen (1 atm of $^{16}O_2$ or $^{18}O_2$) to ferrous LPO at −10 °C, followed by vigorous mixing with a Vortex apparatus for 10 s and then rapid freezing by submersion in liquid nitrogen (77 K). Dithionite reduction is known to exhibit time-dependent spectral changes; for example, the prolonged incubation of ferrous samples results in formation of additional ferrous states.[14] Thus, the rR spectra of ferrous samples (pH 8.5) measured immediately after reduction exhibit a dominant ν(Fe−N_{His}) mode that decreases with time (within 60 min), and a new ν(Fe−N_{His}) band at 221 cm^{-1} appears.[14] In the present work, care was taken to introduce the O_2 and complete mixing within a few minutes, to facilitate formation of the single dioxygen adduct associated with the form exhibiting the ν(Fe−N_{His}) mode at 254 cm^{-1}; that is, the observation of a single ν(Fe−O) mode confirms the presence of a single Compound III. The formation of LPO Compound III was confirmed by acquiring rR spectra at 77 K with the laser power of 1 mW, using the 415 nm excitation line from a Kr ion laser, that is, by inspection of the intensity of the ν(Fe−O) mode at 534 cm^{-1}.

The Cryoradiolytic Reduction. The cryoradiolytic reduction of LPO Compound III samples was done by exposing the samples to 3.5 Mrad of γ-irradiation from a ^{60}Co source at the Notre Dame Radiation Laboratory (University of Notre Dame, South Bend, IN). During irradiation, the samples were contained in a modified Dewar vessel and continuously immersed in the liquid nitrogen. Annealing was done by immersing a given irradiated sample into *n*-pentane/liquid nitrogen solution at a desired temperature for 60 s and then very quickly (<1 s) transferring back into the liquid nitrogen vessel. Temperatures of 170 and 180 K were chosen as appropriate for conversion of peroxo to hydroperoxo forms, based on earlier work with HRP,[26] while a temperature of 200 K was selected to generate the O−O bond cleavage ferryl heme product.[26]

The Resonance Raman Measurements. The resonance Raman spectra of LPO Compound III and Compound 0 were acquired using a Spex 1269 spectrometer equipped with a Spec-10 LN liquid nitrogen-cooled detector (Princeton Instruments, NJ). The data were measured with the 415.4 nm excitation line from a Kr^+ laser (Coherent Innova Sabre Ion Laser). The spectra of irradiated samples annealed at 180 and 200 K, where the O−O bond cleavage product (ferryl heme) is formed, were measured with a 441.6 nm line provided by a He−Cd laser (IK Series He−Cd laser, Kimmon Koha CO., Ltd.), an excitation line that is appropriate for effective enhancement of this species. The rR spectra were collected using back scattering (180°) geometry with the laser beam being focused by a cylindrical lens to form a line image on the sample.[50] The laser power was adjusted to 1 mW or less. All measurements were done at 77 K, and the total collection time was 2 h in the high-frequency region and 2−3 h in the low-frequency region. The slit width was set at 150 μm, and the 1200 g/mm grating was used. The NMR tubes were positioned into a double-walled quartz low temperature cell filled with liquid nitrogen. The sample tubes were spun to avoid local heating. Spectra were calibrated with fenchone (Sigma-Aldrich, WI) and processed with Grams/32 AI software (Galactic Industries, Salem, NH). The difference traces in Figure 7 were deconvoluted using 50/50% Gaussian/Lorentzian functions according to the procedure described in the Supporting Information.

RESULTS

1. LPO Compound III. The rR spectra of the $^{16}O_2$ and $^{18}O_2$ adducts (Compound III) in H_2O and D_2O buffers, at pH 8.2 and 5.6 in the high-frequency region, where heme macrocycle modes occur, are illustrated in Figures S1 and S2 of the Supporting Information. There it is shown that no significant differences are seen in the rR spectra for these two pH values; that is, as expected for a Fe(III)−($O-O^-$) formulation, in both cases the LPO Compound III is in a 6-coordinate low-spin (6cLS) ferric state with identical heme macrocyle structures. These rR spectra are in agreement with previously published data collected at −45 °C with solutions buffered at pH 7.0.[44] It is noted that there were no $^{16}O_2/^{18}O_2$ or H_2O/D_2O-sensitive modes detected in the high-frequency region (bottom two difference traces in Supporting Information Figures S1 and S2). This observation is consistent with the fact that the ν(O−O) stretching mode is commonly not enhanced for histidyl ligated heme protein dioxygen adducts,[51] although some precedent exists for unusual enhancement of these modes in cases where the Fe−O−O fragment is distorted by steric restrictions within the distal pocket (vide infra).[51−53]

On the other hand, the ν(Fe−O) stretching modes of the Fe−O−O fragment of oxygenated heme proteins are typically enhanced, and this behavior is confirmed for these Compound III samples as seen in Figure 3, which presents the low-frequency rR spectra of LPO Compound III at pH 8.2 and their $^{16}O/^{18}O$ difference spectra in both H_2O and D_2O buffers. The

DOI: 10.1021/ja5107833
J. Am. Chem. Soc. 2015, 137, 349−361

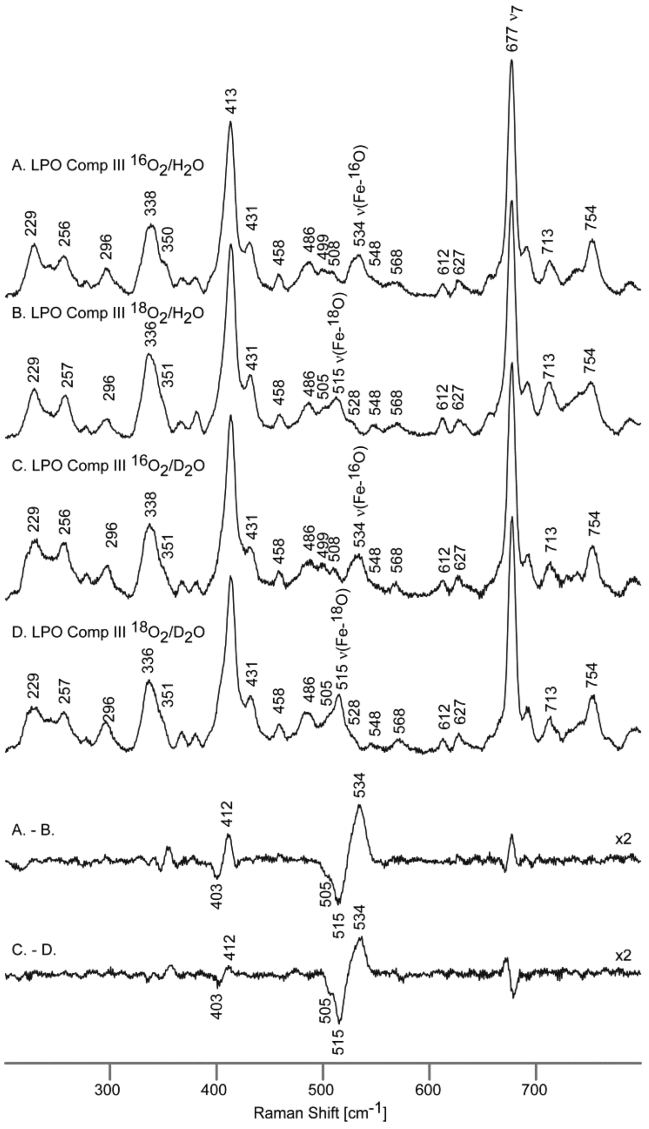

Figure 3. Low-frequency rR spectra of LPO Compound III at pH 8.2, $^{16}O_2/H_2O$ (A), $^{18}O_2/H_2O$ (B), $^{16}O_2/D_2O$ (C), $^{18}O_2/D_2O$ (D), and their difference traces. Spectra measured with 415 nm excitation line at 77 K and normalized to the ν_7 mode at 677 cm^{-1}.

most intense band at 677 cm^{-1} is assigned to the ν_7 heme macrocycle mode, and the modes associated with heme peripheral groups are expected in the region of 330−460 cm^{-1}.[54−57] Most importantly, the oxygen-sensitive modes are observed at 534 and 412 cm^{-1} in the spectra of $^{16}O_2$ in H_2O and D_2O buffers (traces A and C in Figure 3). These modes shift by 19 and 9 cm^{-1} upon $^{18}O_2$ substitution (traces B and D and the difference traces in Figure 3) and are assigned to the ν(Fe−O) stretching and δ(Fe−O−O) bending modes, respectively, noting that (in the absolute spectra) the latter is hidden under the intense 413 cm^{-1} out-of-plane heme mode.[9] On the basis of the two-body harmonic oscillator approximation, the ν(Fe−O) stretching mode should exhibit a 24 cm^{-1} downshift upon ^{18}O substitution. The unusually small apparent $^{16}O_2$−$^{18}O_2$ shift (19 cm^{-1}) observed here has been previously explained by invoking a "Fermi-resonance type interaction"[44,58−60] between the ν(Fe−^{18}O) stretching mode, whose inherent frequency is at 512 cm^{-1}, and the nearby 508 cm^{-1} heme mode, whose inherent frequency is verified by inspection of traces A and C. The vibrational interaction between these two modes results in the upshift of the ν(Fe−^{18}O) mode by 3 cm^{-1} to 515 cm^{-1} and a 3 cm^{-1} downshift of the 508 cm^{-1} mode to 505 cm^{-1}, as can be seen in traces B and D and the difference traces in Figure 3, the derived $^{16}O_2$−$^{18}O_2$ shift (22 cm^{-1}) of the ν(Fe−O) mode being satisfyingly closer to the 24 cm^{-1} calculated shift.

The corresponding spectra of Compound III acquired for solutions at pH 5.6 are presented in Figure 4. Although

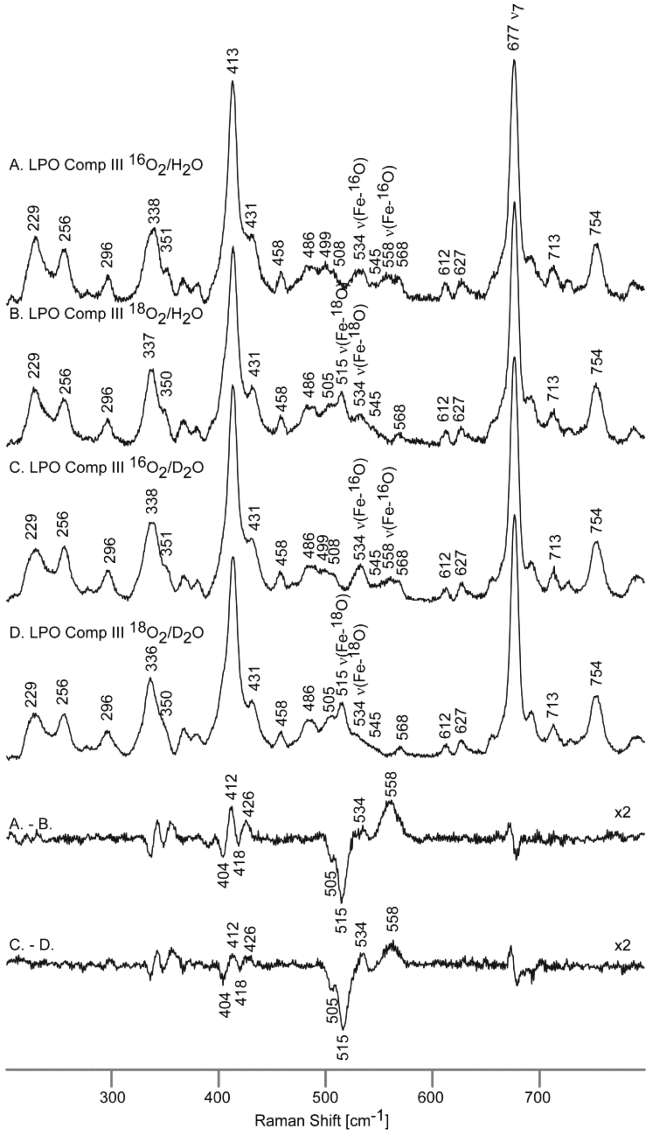

Figure 4. Low-frequency rR spectra of LPO Compound III at pH 5.6, $^{16}O_2/H_2O$ (A), $^{18}O_2/H_2O$ (B), $^{16}O_2/D_2O$ (C), $^{18}O_2/D_2O$ (D), and their difference traces. Spectra measured with 415 nm excitation line at 77 K and normalized to the ν_7 mode at 677 cm^{-1}.

complicated, these new spectral data can be readily understood by first noting that the presence of the 515/505 pair in trace B, along with the 534 cm^{-1} peak in trace A, shows that the species present at pH 8.2 is retained at pH 5.6. However, it is noted that a second form is present, as evidenced by the new 558 cm^{-1} feature seen in trace A, which disappears and apparently is observed at 534 cm^{-1} for the sample prepared with $^{18}O_2$, as shown in trace B; that is, the 534 cm^{-1} feature seen in trace A, assigned to ν(Fe−^{16}O) of the form present at pH 8.2, cannot

DOI: 10.1021/ja5107833
J. Am. Chem. Soc. 2015, 137, 349−361

Table 1. Summary of Frequencies and $^{16}O_2/^{18}O_2$ and H_2O/D_2O Isotopic Shifts for the Oxy, Peroxo, and Hydroperoxo Species of Native Mb and Its Co Substituted Analogues, LPO at Basic and Acidic pH, and Cytochrome P450 and Its D251N Mutant[a]

	frequency and isotopic shift [cm^{-1}]		
	ν(M−O) $\Delta[^{16}O_2/^{18}O_2; H_2O/D_2O]$	ν(O−O) $\Delta[^{16}O_2/^{18}O_2; H_2O/D_2O]$	ref
FeMb			
oxy	578 [−29; 0]		39
peroxo	n.o.		39
hydroperoxo	617 [−25; −5]		39
CoMb			
oxy	549 [−24; 0]	1136 [−68; +2]	41
peroxo	n.o.	n.o.	41
hydroperoxo	583 [−28; −5]	851 [−45; −6]	41
LPO pH 8.2			
oxy	534 [−22; 0]		44, t.w.
peroxo	570 [−22; 0]		t.w.
hydroperoxo	n.o.		t.w.
LPO pH 5.6			
oxy	558 [−24; 0]		t.w.
peroxo	n.o.		t.w.
hydroperoxo	604 [−24; −5]		t.w.
CYP101 WT			
oxy	546 [−31; 0]	1139 [−66; 0]	42
peroxo	n.o.	n.o.	42
hydroperoxo	559 [−27; −3]	799 [−40; −3]	42
CYP101 D251N			
oxy	537 [−30; 0]	1136 [−66; 0] 1125 [−65; +2]	38
peroxo	553 [−27; 0]	792 [−38; 0]	38
hydroperoxo	564 [−28; −2]	774 [−37; −4]	38

[a]n.o., not observed. t.w., this work.

contribute intensity near 534 cm^{-1} for the samples prepared with $^{18}O_2$. Thus, the new form appearing at pH 5.6 exhibits a ν(Fe−^{16}O) mode at 558 cm^{-1} and a ν(Fe−^{18}O) mode at 534 cm^{-1}, a shift that is in good agreement with that calculated for a diatomic oscillator. It is noted that the difference patterns (two bottom traces in Figure 4) at first glance show a confusing ν(Fe−O) difference trace, where there is only one positive ν(Fe−^{16}O) stretching mode at 558 cm^{-1} that is seemingly shifted to the negative 515 cm^{-1} mode, giving an apparent, but quite unreasonable, 43 cm^{-1} downshift. However, this apparent anomaly is easily explained by the assignments described above. Thus, the ν(Fe−^{16}O) mode of the lower frequency Fe−O−O conformer (at 534 cm^{-1}) overlaps with the ν(Fe−^{18}O) mode of the higher frequency Fe−O−O conformer (also at 534 cm^{-1}), resulting in their near cancellation; that is, the intensity of the higher frequency conformer is weaker than that of the lower frequency conformer, so that there is residual positive intensity near 534 cm^{-1}. Finally, it is also noted that the difference patterns (two traces at the bottom of Figure 4) show two sets of the δ(Fe−O−O) bending modes: the 412 cm^{-1} feature that shifts to 404 cm^{-1} in the $^{18}O_2$ sample is identical to that seen previously at pH 8.2 and is associated with the lower frequency Fe−O−O conformer, and a new δ(Fe−O−O) bending mode at 426 cm^{-1}, with a comparable 8 cm^{-1} downshift, that is associated with the higher frequency Fe−O−O conformer.

The frequency of the ν(Fe−O) mode strongly depends on the character of the heme proximal ligand, and for histidine-ligated heme proteins, like LPO and globins, there is an inverse correlation between ν(Fe−N_{His}) and ν(Fe−O_2) modes; that is, the greater is the Fe−N_{His} bond strength (i.e., higher ν(Fe−N_{His}) frequency), the weaker is the Fe−O bond strength (i.e., lower ν(Fe−O_2) frequency).[51,61] Previous rR studies of ferrous LPO revealed that at basic pH (8.5) there are two ν(Fe−N_{His}) modes observed; that is, the dominant one is seen at 254 cm^{-1} and the lower intensity one at 221 cm^{-1}.[14] At pH 5.0, these modes had reversed intensities; the higher frequency 254 cm^{-1} mode has smaller intensity, and the 221 cm^{-1} mode becomes dominant.[14] The ν(Fe−O) stretching mode of Compound III, seen in this present work at basic pH at 534 cm^{-1}, is relatively low as compared to other heme proteins that contain histidine as a proximal ligand, such as myoglobin and hemoglobin (∼572 cm^{-1}); this lowering of the ν(Fe−O) frequency is entirely consistent with the more imidazolate-like character of the proximal histidine, as reflected in the observed high ν(Fe−N_{His}) frequency of 254 cm^{-1}.[62]

In summary of this section, earlier rR studies of LPO had shown that solutions with pH values near 5 contain two forms of ferrous LPO, a dominant form having a relatively weak linkage between the heme iron and the proximal histidine, exhibiting a ν(Fe−N_{His}) frequency of 221 cm^{-1}, and a less populated form possessing a relatively strong linkage, associated with a ν(Fe−N_{His}) frequency of 254 cm^{-1}. At pH 8.5, the same two frequencies were observed, but having opposite relative intensities; that is, now the higher frequency mode was much stronger than that of the 221 cm^{-1} feature. Consistent with those results, in the present work dealing with Compound III derivatives at these widely varying pH values, it is seen that for a low pH value of 5.6, two forms of the dioxygen adduct exist, with a dominant one exhibiting a ν(Fe−O) mode at 558 cm^{-1} and a lower population of a species exhibiting its ν(Fe−O) mode at 534 cm^{-1}. As in the case of the corresponding ferrous derivatives, raising the pH of the Compound III form leads to a

DOI: 10.1021/ja5107833
J. Am. Chem. Soc. 2015, 137, 349−361

reversal of populations, with the 534 cm^{-1} species becoming dominant.

2. LPO Compound 0. On the basis of the results of the relatively few previous rR studies of hydroperoxo derivatives of heme proteins,[38,39,42] the ν(Fe−O) stretching mode of these species is usually observed at ∼25−40 cm^{-1} higher frequency than the corresponding mode of the dioxygen adduct (Compound III) [Table 1]. It is noted that, for the peroxo and hydroperoxo derivatives of globins and other histidyl-ligated heme proteins, the ν(O−O) modes are not generally enhanced. However, in the cases of the peroxo and hydroperoxo derivatives of cytochromes P450, where the trans-axial proximal ligand is thiolate and the associated ν(O−O) modes are resonance enhanced, this mode is observed between 750 and 800 cm^{-1}, a region consistent with a bound peroxo/hydroperoxo fragment. It is further noted that in recent studies of the hydroperoxo derivatives of cobalt-substituted myoglobins,[41] the ν(O−O) modes were also enhanced, an observation consistent with the fact that these modes are strongly enhanced in the corresponding dioxygen adducts of cobalt-substituted myoglobin and hemoglobin.[59,62] Upon careful inspection of the data given in Table 1 for the cytochrome P450 samples, it can be noticed that there exists an inverse correlation between the ν(Fe−O) and ν(O−O) stretching modes; that is, there is a strengthening of the Fe−O bond and attendant weakening of the O−O bond as one proceeds from the dioxygen adduct to the peroxo and then hydroperoxo forms.

Compound 0 at pH 8.2. Returning attention to the present work, first it is noted that, as expected, all irradiated samples are in the ferric low spin state, as judged by positions of oxidation and spin state marker bands seen in the high-frequency region (Supporting Information Figure S3). The low-frequency region of the rR spectra of the samples obtained after γ-ray irradiation of the Compound III samples of LPO at pH 8.2 is shown in Figure 5.

In the spectrum of the $^{16}O_2/H_2O$ sample, a new mode is observed at 570 cm^{-1} that shifts to 548 cm^{-1} for the sample prepared with $^{18}O_2$ (spectrum B), yielding a slightly small isotope shift of only 22 cm^{-1}. (The experimental isotopic shifts of the ν(Fe−O) mode, being small as compared to its calculated shifts, are usually associated with coupling of the ν(Fe−O) mode with underlying heme or proximal trans axial ligand modes (as explained above for Comp III). Another possible explanation of the smaller $^{16}O_2/^{18}O_2$ shift observed here is that it arises from a larger (i.e., more linear) bending angle of the Fe−O−O fragment; e.g., significantly larger isotopic shifts were observed for the dioxygen complex of heme oxygenase (HO) and were attributed to its rather small (heavily bent) Fe−O−O angle.[63]) This 570 cm^{-1} value is 36 cm^{-1} higher than the corresponding Fe−^{16}O stretching mode of Compound III, seen at 534 cm^{-1}, a shift to higher frequency that is consistent with the behavior observed for other peroxo/hydroperoxo heme proteins listed in Table 1, thereby strongly supporting the generation and trapping of a cryoreduced Fe−O−O fragment. The samples in D_2O buffers (traces C and D) exhibit the same spectral pattern as the corresponding samples in H_2O buffer, the lack of an H/D shift prompting the assignment of this species to the ferric peroxo form. It is important to again note that, as in the case of the Compound III species discussed above, there are no $^{16}O_2/^{18}O_2$-sensitive modes observed in the region of 750−800 cm^{-1}, showing that the ν(O−O) modes of the peroxo/hydroperoxo species are not enhanced for this protein.

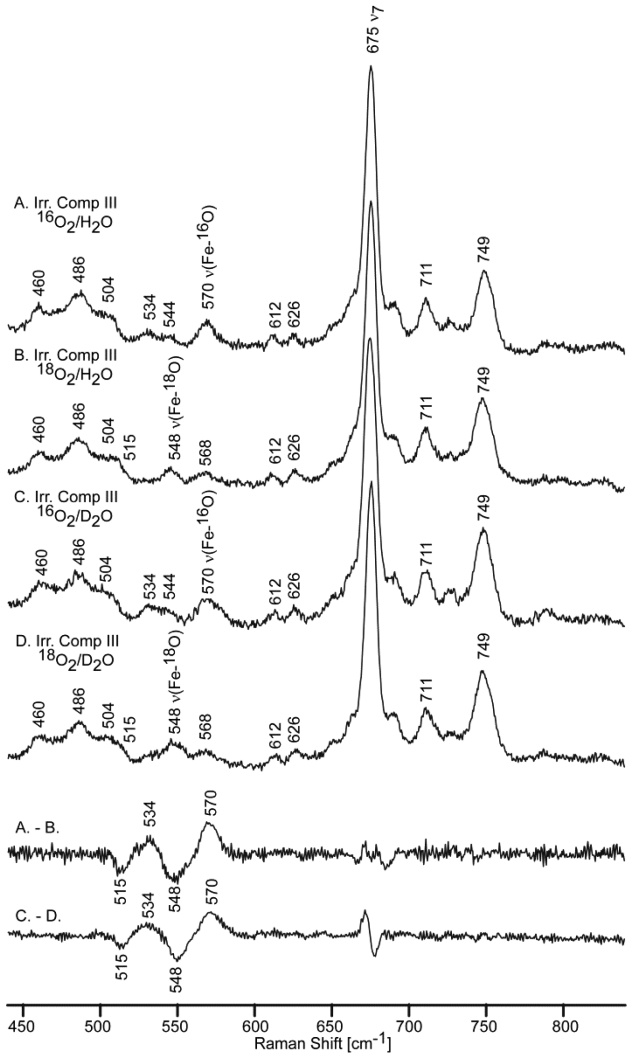

Figure 5. Low-frequency rR spectra of LPO irradiated Compound III at pH 8.2, $^{16}O_2/H_2O$ (A), $^{18}O_2/H_2O$ (B), $^{16}O_2/D_2O$ (C), $^{18}O_2/D_2O$ (D), and their difference traces. Spectra measured with 415 nm excitation line at 77 K and normalized to the ν_7 mode at 675 cm^{-1}.

The additional sets of $^{16}O_2/^{18}O_2$-sensitive modes at 534 cm^{-1} ($^{16}O_2$) and 515 cm^{-1} ($^{18}O_2$) in both H_2O and D_2O buffers (difference traces at the bottom of Figure 5) are associated with residual Compound III precursor (Figure 3), indicating incomplete conversion of Compound III to peroxo/hydroperoxo species in the cryoreduction process. If it is assumed that the relative cross sections for the ν(Fe−O) stretching modes of both Compound III and the peroxo form are the same, the analysis of the difference traces in Figure 3 would indicate that the intensities of positive and negative bands associated with peroxo form have roughly twice the intensity of the corresponding positive and negative bands associated with Compound III, implying that the cryoreduction was ∼60−70% effective. While this estimate is admittedly based on an unexplored assumption, it is also worth making the important point that the precise degree of conversion does not impact the validity of the ν(Fe−O) mode assignment to the peroxo species. Attempts were made to generate the hydroperoxo species by annealing the trapped peroxo species at 170 and 180 K. At 170 K, the intensity of the band assigned to the ν(Fe−O) of the peroxo form had diminished significantly with respect to the 534 cm^{-1} mode of the residual Compound III

DOI: 10.1021/ja5107833
J. Am. Chem. Soc. 2015, 137, 349−361

precursor, with no other ^{18}O-sensitive peaks being observed. In fact, after annealing at 180 K, the mode associated with peroxo species at 570 cm^{-1} had disappeared completely, and only the 534 cm^{-1} ^{18}O-sensitive band of the residual (more stable) Compound III remained; that is, there was no conversion to the hydroperoxo form upon annealing to 180 K, the eventual fate of this ferric peroxo species being discussed later.

Compound 0 at pH 5.6. Having completed an rR spectral characterization of the active site structure of peroxo LPO at elevated pH (8.2), attention was focused on samples prepared under acidic conditions. Before proceeding to discussion of the key features in the low-frequency region, it is first noted that the high-frequency spectral region indicates that all species present in the irradiated and subsequently annealed samples are, as expected, in the ferric low spin state (Supporting Information Figures S3 and S4). Now, focusing on the spectral region wherein the vibrational modes of the Fe−O−O fragment appear, Figure 6 displays rR spectra of irradiated LPO Compound III samples prepared at pH 5.6. Only the stronger intensity bands sensitive to the $^{16}O_2/^{18}O_2$ substitution can be observed in the absolute spectra. Spectrum A shows two

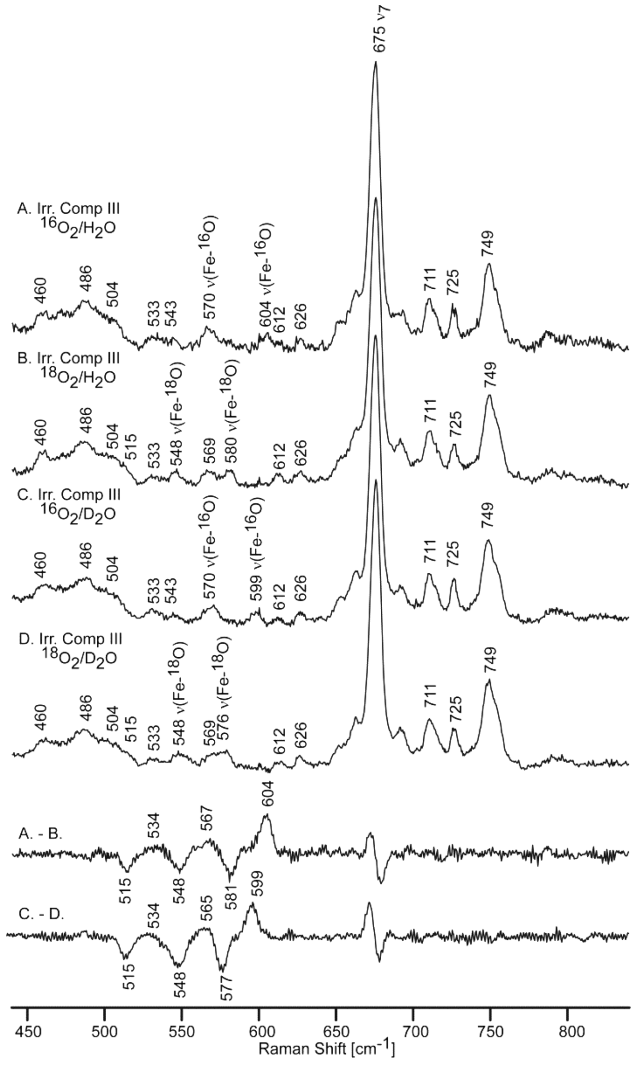

Figure 6. Low-frequency rR spectra of LPO irradiated Compound III at pH 5.6, $^{16}O_2/H_2O$ (A), $^{18}O_2/H_2O$ (B), $^{16}O_2/D_2O$ (C), $^{18}O_2/D_2O$ (D), and their difference traces. Spectra measured with 415 nm excitation line at 77 K and normalized to the ν_7 mode at 675 cm^{-1}.

$^{16}O_2/^{18}O_2$-sensitive features appearing at 570 and 604 cm^{-1} in the spectra of the $^{16}O_2$ adducts that shift upon employing $^{18}O_2$ to 548 and 580 cm^{-1}, respectively (spectrum B). It is noted that only the 604 cm^{-1}/580 cm^{-1} pair of bands is sensitive to H/D exchange (spectra C and D as well as the difference traces A−B vs C−D). However, in addition to these two more obvious pairs of features, the two difference traces of Figure 6 (bottom) show evidence for the presence of other components in the difference patterns, occurring near 534 cm^{-1}/515 cm^{-1}.

These important new, but complex, difference traces are most effectively analyzed with the aid of simulated spectra, as shown in the upper (A) part of Figure 7. The top pattern in the figure exhibits the sets of ($^{16}O_2/^{18}O_2$) paired bands that were needed to produce an overall difference pattern that closely matched the experimental; the experimental and simulated (orange) differences traces are overlaid immediately below the difference trace of simulated components (top trace). While three pairs of bands (red, cyan, and magenta) are obviously present, it is noted that a fourth pair of weak bands (dark blue pair) was required to maximize the fit between simulated and observed difference patterns. All of the derived frequencies are listed in Table 1. Referring to the top set of the derived difference patterns, the highest energy pair exhibits $^{16}O_2/^{18}O_2$ components at 604/581 cm^{-1} (magenta). As seen in Figure 6, this pair exhibits an H/D shift of 4−5 cm^{-1} (i.e., shifting to 599/577 cm^{-1}), consistent with its assignment to hydroperoxo-LPO. The pair of bands seen at 570/548 cm^{-1} (red) is consistent with assignment to peroxo-LPO, exhibiting the same frequencies seen in the cryoreduced samples measured at pH 8.2 with no H/D sensitivity (vide supra). The other two pairs of bands detected, both associated with LPO Compound III, include the weak difference pattern with derived frequencies of 558/534 cm^{-1} (dark blue) and the lowest energy pair having frequencies of 534/515 cm^{-1} (cyan), the last pair corresponding precisely to that seen for LPO Compound III at pH 8.2; it is again noted that the derived ν(Fe−^{18}O) mode is the result of the fitting procedure matching the observed 515 cm^{-1} peak, but it must be recalled that the inherent frequency of this mode is ~512 cm^{-1}, its observed frequency being 515 cm^{-1} due to the interaction with a heme mode whose inherent frequency is close to 508 cm^{-1}.[44,59]

The relative stability of the various forms can be effectively determined by conducting controlled annealing experiments whereby the temperature is raised from 77 K to higher temperatures, noting that the relatively stable Compound III is unlikely to be significantly affected throughout the temperature range spanned here (i.e., 77−200 K). Thus, in Figure 7, the isolated 515 cm^{-1} feature of LPO−$^{18}O_2$ serves as a convenient internal intensity standard throughout the annealing excursion. Referring to the middle two traces (B) in Figure 7, focusing on the upper difference trace of the simulated components, it can be seen that upon raising the temperature from 77 to 170 K, the intensity of the peroxo-LPO mode at 570 cm^{-1} diminishes substantially as compared to that of the hydroperoxo-species (at 604 cm^{-1}), the latter possessing virtually constant intensity at 77 and 170 K, relative to the 515 cm^{-1} internal standard (i.e., 1.00/2.05 vs 1.00/1.98). Furthermore, upon warming to 180 K (Figure 7C), the peroxo-LPO (570 cm^{-1}) disappears completely, while the hydroperoxo-LPO form (at 604 cm^{-1}) has diminished only slightly. The important point to emphasize is that the loss of intensity of the 570 cm^{-1} feature, while maintaining constant relative intensity of the 604 cm^{-1} band until about 180 K, implies that the peroxo species does not

DOI: 10.1021/ja5107833
J. Am. Chem. Soc. 2015, 137, 349−361

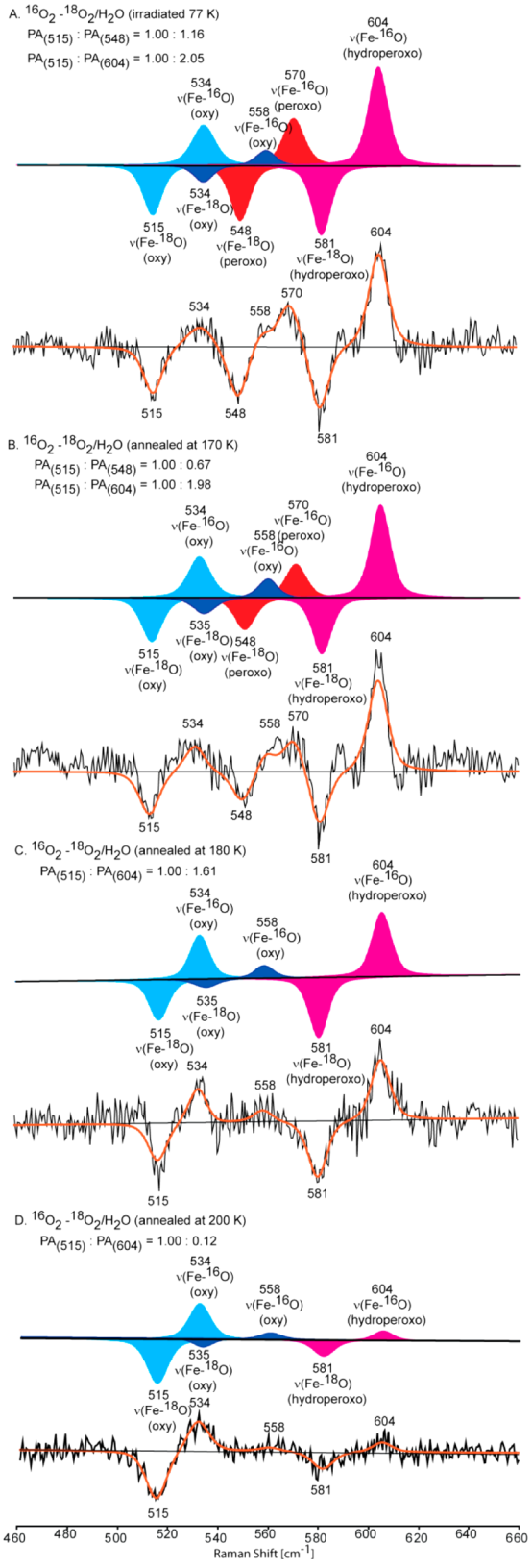

Figure 7. Deconvoluted difference traces ($^{16}O_2$−$^{18}O_2$ in H_2O) of irradiated Compund III at pH 5.6 (A), annealed at 170 K (B), annealed at 180 K (C), and annealed at 200 K (D). The upper parts show corresponding extracted Fe−^{18}O and Fe−^{16}O modes associated with lower frequency Compound III form (cyan), higher frequency Compound III form (dark blue), peroxo form (red), and hydroperoxo form (magenta). The bottom traces show overlapped experimental difference traces (black) with corresponding fitted curve derived from the components shown in the upper part (orange). The $PA_{(515)}$ stands for peak area of mode at 515 cm^{-1} that was used as internal standard used to calculate the changes in peak areas of modes at 548 cm^{-1} (representing peroxo species; $PA_{(548)}$) and 604 cm^{-1} (representing hydroperoxo form; $PA_{(604)}$).

convert to the hydroperoxo (Compound 0) species, but independently converts to a different form, the nature of which is discussed below. Further annealing to 200 K results in almost complete disappearance of the hydroperoxo species (trace D, Figure 7).

Summarizing these results at pH 5.6, a lower frequency mode, seen at 570 cm^{-1} and shifting to 548 cm^{-1} with $^{18}O_2$, corresponds to the ν(Fe−O) stretching mode of the same peroxo form that arises for the sample prepared at pH 8.2, as shown earlier. The 604 cm^{-1} mode is 46 cm^{-1} higher than the new 558 cm^{-1} mode of the Compound III species seen in spectrum A of Figure 4, and in D_2O buffer shifts by 5 cm^{-1} to lower frequency (599 cm^{-1}). This significant H/D sensitivity supports assignment of this 604 cm^{-1} feature to the ν(Fe−O) mode of a new hydroperoxo (Compound 0) species appearing at pH 5.6. As in the cases of the irradiated (pH 8.2) samples discussed earlier, although carefully checked, there are no ($^{16}O_2$−$^{18}O_2$) difference bands observed in the frequency region between ∼750−800 cm^{-1}, where the ν(O−O) stretching modes of peroxo or hydroperoxo fragments would be expected to occur. The rR spectra of the carefully annealed crytotrapped mixture of peroxo-LPO and hydroperoxo-LPO forms demonstrate that the peroxo-LPO does not convert to hydroperoxo-LPO, but decomposes independently throughout the temperature range of 170−180 K, at which point only a small percentage of the hydroperoxo-species has been lost.

3. Ferryl Derivatives Arising from Controlled Annealing To Induce O−O Bond Cleavage Reactions. Having fully documented the appearance and spectral properties of the peroxo and hydroperoxo species in the samples at both pH values, studies were then undertaken to clarify the nature of the products formed upon controlled annealing of these samples. The first sample investigated was the same (pH 5.6) sample annealed at 180 K, whose rR spectrum is shown in Figure 7C. That spectrum showed that the peroxo species (appearing at 570 cm^{-1} at 77 K) was totally depleted at 180 K, while the (Compound 0) hydroperoxo form (604 cm^{-1}) was almost completely retained. As can be seen in Figure 8, top trace, using the 441.6 nm excitation line, which is known to efficiently enhance Raman lines of the ferryl species, the lost peroxo form has been converted to a ferryl heme species, whose 747 cm^{-1} observed frequency (shifting to 715 cm^{-1} upon $^{18}O_2$ substitution) is entirely consistent with the previously assigned ν(Fe═O) stretching frequency of the ferryl derivative of LPO in aqueous buffer.[64] It is noted that this frequency is also consistent with a strong trans-axial Fe−N_{His} linkage in its ferrous form. Thus, the peroxo form that had disappeared by 180 K and the ferryl form that had formed by 180 K are both associated with a strong trans-axial histidine linkage, that is, ∼254 cm^{-1}.[14]

As is seen in the traces in the bottom half of Figure 8, upon annealing to 200 K, a new set of $^{16}O/^{18}O$-sensitive modes with components at 783 and ∼748 cm^{-1} appears in addition to the initially formed 747/715 cm^{-1} component. The difference trace

DOI: 10.1021/ja5107833
J. Am. Chem. Soc. 2015, 137, 349−361

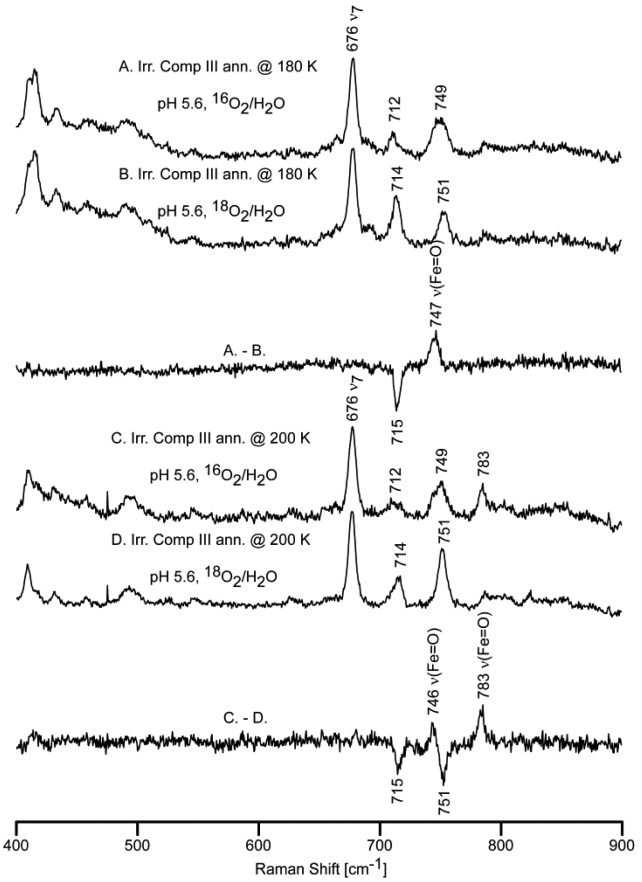

Figure 8. Low-frequency rR spectra of irradiated LPO Compound III (pH 5.6) annealed at 180 K $^{16}O_2/H_2O$ (A) and $^{18}O_2/H_2O$ (B) and annealed at 200 K $^{16}O_2/H_2O$ (C) and $^{18}O_2/H_2O$ (D). The $^{16}O_2-^{18}O_2$ difference traces are shown directly under absolute spectra. Spectra were measured with 441.6 nm excitation line and normalized to the ν_7 mode at 676 cm^{-1}. The spectra shown here were acquired for the same samples used to generate the difference traces in Figure 7C; that is, the samples contain both the ferryl and the hydroperoxo species, but only the ferryl form is effectively in resonance with the 441.6 nm excitation line, noting that relative enhancement of heme modes may vary from derivative to derivative and with different excitation lines.

shown at the bottom reveals a pattern that is consistent with partial cancellation of the ν(Fe=^{18}O) mode of the higher frequency set with the ν(Fe=^{16}O) mode of the lower frequency component. This higher frequency set of modes, with its ν(Fe^{16}=O) frequency of 783 cm^{-1}, is quite consistent with that expected for a ferryl heme bearing a relatively weak trans-axial Fe–N_{His} linkage, the species with a ν(Fe–N_{His}) frequency of 221 cm^{-1} dominating the spectrum for ferrous LPO at pH = 5; that is, ν(Fe=^{16}O) values of between 780 and 800 cm^{-1} are typically observed for heme proteins whose ν(Fe–N_{His}) varies from ~240 to 220 cm^{-1}.[14] Finally, it is noted that for comparable studies conducted for the isolated peroxo species trapped at pH 8.2, where there exists a paucity of mobile protons, no evidence is obtained for a ferryl species, the expected product of O–O bond cleavage. Apparently, in the absence of an adequate supply of protons, the ferric peroxo species decomposes by an as yet undetermined mechanism; further studies, employing a wider range of conditions and a larger number of resonance excitation lines, are planned for the future.

DISCUSSION

Faced with the difficulties encountered with rapid mixing methods to trap the elusive Compound 0 enzymatic intermediate of mammalian peroxidases for definitive structural characterization, here cryoradiolytic reduction of the trapped ferrous dioxygen adduct, Compound III, is employed to generate the peroxo- and hydroperoxo-LPO (Compound 0) species, the relative populations of which depend on the pH. Controlled annealing procedures are used to isolate peroxo and hydroperoxo species and to induce O–O bond cleavage, producing the ferryl heme intermediates. Resonance Raman spectroscopy is used to identify and characterize the Fe–O–O and Fe–O–O–H fragments of the Compound III, peroxo, and Compound 0 intermediates, as well as the ν(Fe=O) of the ferryl heme O–O bond cleavage products. Comparison of acquired data reveals quite dramatic effects of pH on the relative strengths of the Fe–O and Fe=O bonds of these species, thereby permitting a more rational interpretation of the corresponding effects on the reactivity of these species.

Alternate Forms of Compound III. As described earlier in discussing the reaction sequence depicted in Figure 2, the distal histidine His109 is typically assigned a pK_a value of 5.8–6.4,[15,65] implying that for the studies conducted here at pH 8.2, one would expect that the population of LPO molecules bearing a nonprotonated His109 would strongly dominate. Indeed, the rR spectral data provide clear evidence that only one Compound III form, exhibiting its ν(Fe–^{16}O) mode at 534 cm^{-1}, is observed. The spectra of the samples prepared at pH 5.6, on the other hand, demonstrate that a second form of Compound III is present, exhibiting its ν(Fe–^{16}O) mode at 558 cm^{-1}, signaling a significant increase in the strength of the Fe–O bond relative to the species seen at alkaline pH. While it is tempting to ascribe this behavior to H-bond donation by the protonated distal His109 residue to the Fe–O–O fragment of Compound III based on results from previously published work for dioxygen adducts of other heme proteins,[38,51,66–68] it is difficult to accept a suggested H-bond donor effect of this magnitude on the ν(Fe–O) mode. For example, in the case of dioxygen adducts of myoglobin, where the distal histidine was removed, only slight (<5 cm^{-1}) shifts of the ν(Fe–O) mode were seen relative to WT Mb.[51,66] Similarly, comparison of a series of cytochrome P450 dioxygen adducts with varying degrees of distal side H-bonding configurations, including some with H-bond donating substrates, shows that shifts of the ν(Fe–O) mode attributable to the H-bonding interaction are typically in the neighborhood of only 5–10 cm^{-1}, with an interesting and very informative detail being that the shift for H-bonding to the terminal oxygen in the Fe–O–O fragment induces upshifts in ν(Fe–O), while H-bonding to the proximal oxygen caused downshifts of similar magnitude.[38,51,67,68]

Given these reservations about ascribing the unexpectedly large positive shifts of the ν(Fe–O) mode solely to distal side interactions, further consideration was given to possible pH-induced alterations of proximal side architecture that might account for these vibrational data. Fortunately, a directly relevant and carefully conducted study on the impact of pH changes on the heme-proximal histidine linkage of LPO offers some useful insight.[14] In that work, Smulevich, Obinger, and co-workers show that two ν(Fe–N_{His}) stretching modes are observed, appearing at 221 and 254 cm^{-1}, whose relative intensities are pH dependent, with the 254 cm^{-1} feature dominating at high pH (8.5) and the 221 cm^{-1} band

DOI: 10.1021/ja5107833
J. Am. Chem. Soc. 2015, 137, 349–361

dominating at low pH (5.0). Those authors point out that, while the protonation status of the proximal histidine undoubtedly plays a crucial role in modulating the donor strength, with an "imidazolate" formulation being applicable at alkaline pH, other factors, including reorientation of the imidazole plane with respect to the four Fe−N bonds of the heme macrocycle, brought about by structural rearrangements within the heme pocket, could also alter the strength of the Fe−N_{His} linkage. In any case, the observed variation of the ν(Fe−N_{His}) as a function of pH is an important finding, because there exists a well-documented inverse correlation between the frequency (bond strength) of the ν(Fe−N_{His}) mode of the ferrous form and the ν(Fe−O) frequencies of various oxy forms of heme proteins.[51,61]

The potential influence of this correlation in determining the status of the trans-axial Fe−O linkages in the present case is outlined in Figure 9. At alkaline pH (8.2), the species

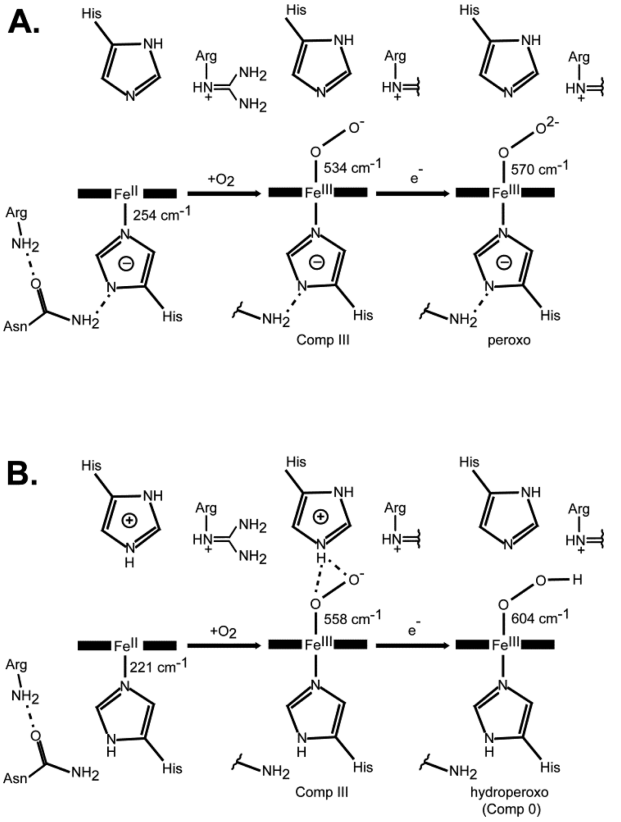

Figure 9. Mechanism of formation of Compound III at basic (A) and acidic (B) pH and their transition to peroxo (A) and hydroperoxo (Compound 0) (B) forms.

possessing the strong Fe−N_{His} bond, with its ν(Fe−N) mode of 254 cm^{-1}, dominates and is correlated with the Compound III form possessing a relatively weak Fe−O bond, whose ν(Fe−O) mode occurs at 534 cm^{-1}. Under acidic conditions (pH 5.6), a second ferrous LPO species, with a relatively weak Fe−N_{His} bond exhibiting its ν(Fe−N_{His}) mode at 221 cm^{-1},[14] is also present and forms a Compound III species whose ν(Fe−O) mode occurs at 558 cm^{-1}. It is also important to point out that this new Compound III species formed in acidic conditions not only possesses a weakened trans-axial Fe−N_{His} linkage, but also presumably houses an Fe−O−O fragment that is involved in an H-bonding interaction with a protonated His109, the influence of which on its ν(Fe−O) frequency would depend on whether the H-bond forms between the proximal or terminal oxygen atom of the Fe−O−O fragment.[51,67] To the extent that deoxyMb and this low-pH form of ferrous LPO both possess similar Fe−N_{His} bond strengths, as evidenced by similar ν(Fe−N_{His}) stretching frequencies of ∼221 cm^{-1}, it would be expected that both would exhibit similar ν(Fe−O) frequencies in the corresponding dioxygen adducts, yet these differ by ∼16 cm^{-1} (558 cm^{-1} for frozen LPO Compound III and 574 cm^{-1} for frozen oxyMb).[39,41,56] Given the fact that the Fe−O−O fragment of oxyMb is known to be stabilized by an H-bonding interaction between the terminal oxygen and a distal pocket histidyl imidazole group that would lead to an increase in the inherent ν(Fe−O) frequency, the 558 cm^{-1} frequency observed here for the low-pH form of LPO Compound III could suggest that the H-bonding interaction of the protonated distal His109 is either not properly oriented to interact with the terminal oxygen or may even be positioned to interact with the proximal oxygen atom of the Fe−O−O fragment, the latter situation being known to cause negative shifts of the ν(Fe−O) mode, as was clearly seen for the dioxygen adduct CYP17 in the presence of hydroxy pregnenolene.[67] However, although possible alignment of the His109 H-bond with the proximal oxygen of the Fe−O−O fragment is consistent with the data for this Compound III form, the data for the corresponding Compound 0 derivative formed upon cryoreduction are entirely consistent with the expected hydroperoxo LPO formulation (vide infra).

Characterization and Fate of Compound 0 and Peroxo LPO. Cryoreduction of Compound III under alkaline conditions produced only peroxo LPO, with an ν(Fe−^{16}O) frequency at 570 cm^{-1} that, as expected, is not sensitive to exchange of H_2O with D_2O (Figure 9). This frequency shift of 36 cm^{-1} to higher frequency upon conversion of LPO Compound III to its peroxo derivative is in reasonable agreement with that expected from consideration of previously acquired rR data for globins,[69] where the ν(Fe−O) mode for the dioxygen adduct occurs near 578 cm^{-1} while that for the corresponding peroxo derivative occurs near 606 cm^{-1}. Interestingly, annealing of this frozen solution of trapped peroxo LPO at 180 K leads only to loss of the 570 cm^{-1} feature without producing any new $^{16}O_2/^{18}O_2$-sensitive features with excitation at 415 nm, thereby demonstrating that conversion to the hydroperoxo form, compound 0, does not occur under alkaline conditions; that is, in this situation, proton delivery to the heme active site is apparently quite inefficient due to the very low concentration of protons. In line with this observation is the fact that interrogation of the annealed sample using 441.6 nm excitation, where any ferryl heme would be detected, failed to yield any $^{16}O/^{18}O$-sensitive features. A rather extensive amount of further work will be required to clarify the fate of the lost peroxo form.

As shown in Figure 6 and described above, cryoreduction of Compound III of LPO in frozen solutions under acidic conditions at pH 5.6 produces a new feature observed at 604 cm^{-1}, which shifts by 5 cm^{-1} to lower frequency in solutions prepared in D_2O, a result that is consistent with its assignment to Compound 0. With the precursor (Compound III form) possessing a protonated distal His109 at pH 5.6 and a ν(Fe−^{16}O) mode at 558 cm^{-1}, the resultant shift of 46 cm^{-1} upon converting from Compound III to Compound 0 is reasonably consistent with the corresponding shift seen for globins, where the ν(Fe−O) mode of oxyMb shifted from 578

DOI: 10.1021/ja5107833
J. Am. Chem. Soc. 2015, 137, 349−361

to 617 cm^{-1} for hydroperoxo Mb.[39−41] Thus, it is seen that at pH 5.6, two distinct populations of cryoreduced species exist, peroxo and hydroperoxo, an observation consistent with two populations of each precursor; that is, ferrous LPO exhibited a dominant $\nu(Fe-N_{His})$ mode at 221 cm^{-1} and a weaker one at 254 cm^{-1}, while the two populations of LPO Compound III were confirmed by a strong $\nu(Fe-O)$ mode at 558 cm^{-1} and a weak one observed at 534 cm^{-1}, the latter being associated with the (less populated) form having an imidazolate-like proximal histidine with a $\nu(Fe-N_{His})$ mode of 254 cm^{-1}.

Before turning attention to the fate of these peroxo and hydroperoxo forms upon further annealing, it is interesting to consider the implications of these findings under acidic conditions with respect to the issue of proton delivery to the bound peroxo-fragment. The rR spectra of the Compound III sample (Figure 4) exhibited evidence for a non-H-bonded form ($\nu(Fe-^{16}O)$ = 534 cm^{-1}) and an H-bonded form ($\nu(Fe-^{16}O)$ = 558 cm^{-1}), the source of the H-bond being most reasonably ascribed to protonated His109. Upon cryoreduction, without further annealing above 77 K, two reduced forms are detected, a peroxo species and an H/D-sensitive hydroperoxo species. Now, on the basis of consideration of shifts typically observed in conversion from dioxy to peroxo/hydroperoxo forms, as well as the observation of the telltale shift observed upon deuteration of hydroperoxo forms, the most reasonable interpretation of the rR spectral data acquired for irradiated samples is that the resulting Compound 0 form, with a $\nu(Fe-^{16}O)$ = 604 cm^{-1}, is derived by direct and quite efficient proton transfer from the protonated His109 to an initially formed transient peroxo-species. This conclusion receives support from consideration of many previous cryoradiolysis studies, wherein it is generally possible to trap the peroxo forms at 77 K before accessing the hydroperoxo form by annealing at higher temperatures, the implication being that facile proton transfer at 77 K is likely to originate only from an H-bond donor group within the distal pocket. Clearly, this argument is further supported by the fact that the trapped peroxo-form in this same sample, which arose from reduction of the non-H-bonded Compound III, remained unprotonated at 77 K due to the lack of an effective active site proton donor. Although the above considerations effectively argue for protonation of the terminal oxygen atom of the Fe−O−O fragment by protonated His109, it is noted that a recently published study of a different peroxidase, cytochrome c peroxidase (ccp), employing neutron diffraction methods for the ferric and ferryl species, presents effective arguments that (in that enzyme) the protonation of the hydroperoxo species (Compound 0) involves a different distal pocket residue, probably a protonated arginine (Arg48), with the distal histidine remaining protonated following Compound I formation.[70] Assuming those results and arguments are esentially correct, the difference from the present work on LPO and those studies on ccp may arise from the fact that in the latter work the proton transfer being dealt with is that of the key "catalytic" proton to the actual Compound 0, while that being addressed in the present work is a proton transfer step to form a trapped Compound 0 species for structural characterization.

Having defined the nature and relative populations of the peroxo and hydroperoxo forms trapped at 77 K under acidic conditions, it remains only to consider their relative stability as reflected by their behavior observed upon controlled annealing. As seen in Figure 7, annealing of this sample resulted in loss of the peroxo-LPO content of the sample before any substantial loss of the Compound 0. Inspection of Figure 8 provides definitive evidence that the peroxo fragment converted to a ferryl species with a $\nu(Fe-^{16}O)$ at 747 cm^{-1}; that is, both the peroxo form and the resultant ferryl form are associated with the population of LPO having a strong $Fe-N_{His}$ bond, with a $\nu(Fe-N_{His})$ of 254 cm^{-1}. During this process, the Compound 0 form, with its weaker trans-axial histidyl ligand, does not undergo O−O bond cleavage. Indeed, the O−O bond cleavage for the hydroperoxide form associated with the weaker $Fe-N_{His}$ bond occurs only at 200 K. The most reasonable interpretation of this behavior is that upon annealing to higher temperatures, where protons become more mobile and enter the active site, the stronger "push effect" of the imidazolate-like form substantially increases the efficiency of the O−O bond cleavage process. While the population expressing a strong push effect is depleted by 180 K, the population possessing the weaker $Fe-N_{His}$ linkage was seen to undergo substantial O−O bond cleavage only at 200 K, the difference in O−O bond cleavage efficiency, as documented spectroscopically herein for the first time, directly reflecting the dominant influence of the "push" effect relative to the "pull" effect.[71,72]

Early work by Kimura and Yamazaki[73] confirming even earlier work by Dunford and co-workers[74] shows the rate of the reaction is pH independent between about 5 and 11, the rate decreasing relatively sharply below pH 5, results that are most reasonably attributed to protonation of the distal histidine, which would in turn hamper the required deprotonation of the incoming H_2O_2, presumably the rate-limiting step. While at pH values between 5 and 9, there are apparently different populations of LPO having weak and stronger $Fe-N_{His}$ linkages (based on the rR data in ref 14), the corresponding effects on the rate of Compound I formation are small relative to the effect of distal side protonation. In the present work, to capture the peroxo/hydroperoxo intermediates, the reactive $Fe(III)-(O-O^{2-})$ and $Fe(III)-(O-OH^{-})$ fragments are generated without permitting delivery of a "catalytic" proton. This approach permits the determination of the effects of proximal side differences on the efficiencies of O−O bond cleavage, such differences being masked in solution phase work by the slowness of the primary H_2O_2 binding step. Further definition of these processes will require more highly resolved pH variations and additional annealing temperatures (i.e., between 77 and 180 K), whereupon it is anticipated that a new hydroperoxo species will emerge, exhibiting a $\nu(Fe-O)$ frequency between 580 and 590 cm^{-1}.

Finally, one of the key findings of the present work is the demonstration of an essential difference between mammalian peroxidases from their counterparts in plants. In the latter case, it is known that the strength of the $Fe-N_{His}$ bond is affected only slightly by variations in pH between ∼5−11, as reflected in small (<5 cm^{-1}) changes in the $\nu(Fe-N_{His})$ frequencies.[75] On the other hand, as is seen here, the pH-induced changes in the $\nu(Fe-N_{His})$ lead to substantial changes in the strengths of the Fe−O bonds of the Compound III and all subsequent Fe−O−O and Fe=O intermediates, effects that clearly hold implications for differences in the complex reactivity patterns of these mammalian enzymes.[11,12,17,18]

■ ASSOCIATED CONTENT

Supporting Information

Description of the deconvolution procedure, and high-frequency spectra of Compound III and its irradiated form at

DOI: 10.1021/ja5107833
J. Am. Chem. Soc. 2015, 137, 349−361

basic and acidic pH. This material is available free of charge via the Internet at http://pubs.acs.org.

AUTHOR INFORMATION

Corresponding Author

james.kincaid@mu.edu

Notes

The authors declare no competing financial interest.

ACKNOWLEDGMENTS

This work was supported by a grant from the National Science Foundation (MCB 0951110) to J.R.K. We gratefully appreciate help provided by Dr. Jay A. LaVerne and Dr. John Bentley, Notre Dame Radiation Laboratory (Notre Dame University, IN), a facility of the U.S. Department of Energy, Office of Basic Energy Science. We wish to thank the owners of Crane Dairy Farms, Burlington, WI, for the gift of cows' milk.

REFERENCES

(1) Pruitt, K.; Tenovuo, J. *The Lactoperoxidase System: Chemistry and Biological Significance*; Marcel Dekker: New York, 1985.

(2) Reiter, B.; Perraudin, J. P. In *Peroxidases in Chemistry and Biology*; Everse, J., Everse, K. E., Grisham, M. B., Eds.; CRC Press: Boca Raton, FL, 1991; Vol. *1*, pp 143−180.

(3) Poulos, T. L. *Arch. Biochem. Biophys.* **2010**, *500*, 3−12.

(4) Singh, A. K.; Singh, N.; Sharma, S.; Singh, S. B.; Kaur, P.; Bhushan, A.; Srinivasan, A.; Singh, T. P. *J. Mol. Biol.* **2008**, *376*, 1060−1075.

(5) Singh, A. K.; Singh, N.; Sharma, S.; Shin, K.; Takase, M.; Kaur, P.; Srinivasan, A.; Singh, T. P. *Biophys. J.* **2009**, *96*, 646−654.

(6) Andersson, L. A.; Bylkas, S. A.; Wilson, A. E. *J. Biol. Chem.* **1996**, *271*, 3406−3412.

(7) Rae, T. D.; Goff, H. M. *J. Biol. Chem.* **1998**, *273*, 27968−27977.

(8) Hu, S.; Treat, R. W.; Kincaid, J. R. *Biochemistry* **1993**, *32*, 10125−10130.

(9) Zbylut, S. D.; Kincaid, J. R. *J. Am. Chem. Soc.* **2002**, *124*, 6751−6758.

(10) Brogioni, S.; Feis, A.; Marzocchi, M. P.; Zederbauer, M.; Furtmuller, P. G.; Obinger, C.; Smulevich, G. *J. Raman Spectrosc.* **2006**, *37*, 263−276.

(11) Carpena, H.; Vidossich, P.; Schroettner, K.; Calisto, B. M.; Banerjee, S.; Stampler, J.; Soudi, M.; Furtmüller, P. G.; Rovira, C.; Fita, I.; Obinger, C. *J. Biol. Chem.* **2009**, *284*, 25929−25937.

(12) Poulos, T. L. *Chem. Rev.* **2014**, *114*, 3919−3962.

(13) Teraoka, J.; Kitagawa, T. *J. Biol. Chem.* **1981**, *256*, 3969−3977.

(14) Brogioni, S.; Stampler, J.; Furtmueller, P. G.; Feis, A.; Obinger, C.; Smulevich, G. *Biochim. Biophys. Acta* **2008**, *1784*, 843−849.

(15) Monzani, E.; Gatti, A. L.; Profumo, A.; Casella, L.; Gullotti, M. *Biochemistry* **1997**, *36*, 1918−1926.

(16) Ghibaudi, E.; Laurenti, E. *Eur. J. Biochem.* **2003**, *270*, 4403−4412.

(17) Jantschenko, W.; Furtmuller, P. G.; Zederbauer, M.; Neugschwandtner, K.; Jakopitsch, C.; Obinger, C. *Arch. Biochem. Biophys.* **2005**, *434*, 51−59.

(18) Furtmüller, P. G.; Zederbauer, M.; Jantschko, W.; Helm, J.; Bogner, M.; Jakopitsch, C.; Obinger, C. *Arch. Biochem. Biophys.* **2006**, *445*, 199−213.

(19) Fielding, A. J.; Singh, R.; Boscolo, B.; Loewen, P. C.; Ghibaudi, E. M.; Ivancich, A. *Biochemistry* **2008**, *47*, 9781−9792.

(20) Beak, H. K.; Van Wart, H. E. *Biochemistry* **1989**, *28*, 5714−5719.

(21) Beak, H. K.; Van Wart, H. E. *J. Am. Chem. Soc.* **1992**, *114*, 718−725.

(22) Shintaku, M.; Matsuura, K.; Yoshioka, S.; Takahashi, S.; Ishimori, K.; Morishima, I. *J. Biol. Chem.* **2005**, *280*, 40934−40938.

(23) Kappl, R.; Hoehn-Berlage, M.; Huettermann, J.; Bartlett, N.; Symons, M. C. R. *Biochim. Biophys. Acta* **1985**, *827*, 327−343.

(24) Davydov, R.; Perera, R.; Jin, S.; Yang, T.-C.; Bryson, T. A.; Sono, M.; Dawson, J. H.; Hoffman, B. M. *J. Am. Chem. Soc.* **2005**, *127*, 1403−1413.

(25) Denisov, I. G.; Grinkova, Y. V.; Sligar, S. G. *Methods Mol. Biol.* **2012**, *875*, 375−391.

(26) Denisov, I. G.; Makris, T. M.; Sligar, S. G. *J. Biol. Chem.* **2002**, *277*, 42706−42710.

(27) Davydov, R.; Osborne, R. L.; Shanmugam, M.; Du, J.; Dawson, J. H.; Hoffman, B. M. *J. Am. Chem. Soc.* **2010**, *132*, 14995−15004.

(28) Davydov, R.; Makris, T. M.; Kofman, V.; Werst, D. E.; Sligar, S. G.; Hoffman, B. M. *J. Am. Chem. Soc.* **2001**, *123*, 1403−1415.

(29) Gantt, S. L.; Denisov, I. G.; Grinkova, Y. V.; Sligar, S. G. *Biochem. Biophys. Res. Commun.* **2009**, *387*, 169−173.

(30) Davydov, R.; Razeghifard, R.; Im, S.-C.; Waskell, L.; Hoffman, B. M. *Biochemistry* **2008**, *47*, 9661−9666.

(31) Davydov, R.; Gilep, A. A.; Strushkevich, N. V.; Usanov, S. A.; Hoffman, B. M. *J. Am. Chem. Soc.* **2012**, *134*, 17149−17156.

(32) Kuhnel, K.; Derat, E.; Terner, J.; Shaik, S.; Schlichting, I. *Proc. Natl. Acad. Sci. U.S.A.* **2007**, *104*, 99−104.

(33) Schlichting, I.; Berendzen, J.; Chu, K.; Stock, A. M.; Maves, S. A.; Benson, D. E.; Sweet, R. M.; Ringe, D.; Petsko, G. A.; Sligar, S. G. *Science* **2000**, *287*, 1615−1622.

(34) Hersleth, H.-P.; Hsiao, Y.-W.; Ryde, U.; Görbitz, C. H.; Andersson, K. K. *Biochem. J.* **2008**, *412*, 257−264.

(35) Sawai, H.; Sugimoto, H.; Kato, Y.; Asano, Y.; Shiro, Y.; Aono, S. *J. Biol. Chem.* **2009**, *284*, 32089−32096.

(36) Beitlich, T.; Kühnel, K.; Schulze-Briese, C.; Shoeman, R. L.; Schlichting, I. *J. Synchrotron Radiat.* **2007**, *14*, 11−23.

(37) G. Keilin, D.; Hartree, E. F. *Biochem. J.* **1951**, *49*, 88−104.

(38) Denisov, I. G.; Mak, P. J.; Makris, T. M.; Sligar, S. G.; Kincaid, J. R. *J. Phys. Chem. A* **2008**, *112*, 13172−13179.

(39) Ibrahim, M.; Denisov, I. G.; Makris, T. M.; Kincaid, J. R.; Sligar, S. G. *J. Am. Chem. Soc.* **2003**, *125*, 13714−13718.

(40) Ibrahim, M.; Kincaid, J. R. *J. Porphyrins Phthalocyanines* **2004**, *8*, 215−225.

(41) Mak, P. J.; Kincaid, J. R. *J. Inorg. Biochem.* **2008**, *102*, 1952−1957.

(42) Mak, P. J.; Denisov, I. G.; Victoria, D.; Makris, T. M.; Deng, T.-J.; Sligar, S. G.; Kincaid, J. R. *J. Am. Chem. Soc.* **2007**, *129*, 6382−6383.

(43) Malle, E.; Furtmuller, P. G.; Sattler, W.; Obinger, C. *Br. J. Pharmacol.* **2007**, *152*, 838−854.

(44) Hu, S.; Kincaid, J. R. *J. Am. Chem. Soc.* **1991**, *113*, 7189−7194.

(45) Poulos, L. P.; Kraut, J. *J. Biol. Chem.* **1980**, *255*, 8199−8205.

(46) Morrison, M. *Methods Enzymol.* **1970**, *17*, 653−657.

(47) Goff, H. M.; Gonzalez-Vergara, E.; Ales, D. C. *Biochem. Biophys. Res. Commun.* **1985**, *133*, 794−799.

(48) Ferrari, R. P.; Laurenti, E.; Cecchini, P. I.; Gambino, O.; Sondergaard, I. *J. Inorg. Biochem.* **1995**, *58*, 109−127.

(49) Tolmachey, Y. V.; Wang, Z.; Hu, Y.; Bae, I. T.; Scherson, D. A. *Anal. Chem.* **1998**, *70*, 1149−1155.

(50) Shriver, D. F.; Dunn, J. B. R. *Appl. Spectrosc.* **1974**, *28*, 319−323.

(51) Spiro, T. G.; Soldatova, A. V.; Balakrishnan, G. *Coord. Chem. Rev.* **2013**, *257*, 511−527.

(52) Das, T. K.; Couture, M.; Ouellet, Y.; Guertin, M.; Rousseau, D. L. *Proc. Natl. Acad. Sci. U.S.A.* **2001**, *98*, 479−484.

(53) Takahashi, S.; Ishikawa, K.; Takeuchi, N.; Ikeda-Saito, M.; Yoshida, T.; Rousseau, D. L. *J. Am. Chem. Soc.* **1995**, *117*, 6002−6006.

(54) Hu, S.; Smith, K. M.; Spiro, T. G. *J. Am. Chem. Soc.* **1996**, *118*, 12638−12646.

(55) Chen, Z.; Ost, T. W. B.; Schelvis, J. P. M. *Biochemistry* **2004**, *43*, 1798−1808.

(56) Mak, P. J.; Podstawka, E.; Kincaid, J. R.; Proniewicz, L. M. *Biopolymers* **2004**, *75*, 217−228.

(57) Cerda-Colon, J. F.; Silfa, E.; Lopez-Garriga, J. *J. Am. Chem. Soc.* **1998**, *120*, 9312−9317.

(58) Fermi, E. *Z. Phys.* **1931**, *71*, 250−259.

(59) Proniewicz, L. P.; Kincaid, J. R. *Coord. Chem. Rev.* **1997**, *161*, 81−127.

(60) Veas, C.; McHale, J. L. *J. Am. Chem. Soc.* **1989**, *111*, 7042−7046.

DOI: 10.1021/ja5107833
J. Am. Chem. Soc. 2015, 137, 349−361

(61) Oertling, W. A.; Kean, R. T.; Wever, R.; Babcock, G. T. *Inorg. Chem.* **1990**, *29*, 2633−2645.
(62) Bruha, A.; Kincaid, J. R. *J. Am. Chem. Soc.* **1988**, *110*, 6006−6014.
(63) Takahashi, S.; Ishikawa, K.; Takeuchi, N.; Ikeda-Saito, M.; Yoshida, T.; Rousseau, D. L. *J. Am. Chem. Soc.* **1995**, *117*, 6002−6006.
(64) Reczek, C. M.; Sitter, A. J.; Terner, J. *J. Mol. Struct.* **1989**, *214*, 27−41.
(65) Modi, S.; Behere, D. V.; Mitra, S. *Biochemistry* **1989**, *28*, 4689−4694.
(66) Hirota, S.; Li, T.; Phillips, G. N., Jr.; Olson, J. S.; Mukai, M.; Kitagawa, T. *J. Am. Chem. Soc.* **1996**, *118*, 7845−7846.
(67) Gregory, M.; Mak, P. J.; Sligar, S. G.; Kincaid, J. R. *Angew. Chem., Int. Ed.* **2013**, *52*, 5342−5345.
(68) Tosha, T.; Kagawa, N.; Arase, M.; Waterman, M. R.; Kitagawa, T. *J. Biol. Chem.* **2008**, *283*, 3708−3717.
(69) Mak, J. P.; Kincaid, J. R., unpublished results.
(70) H. Casadei, C. M.; Gumiero, A.; Metcalfe, C. L.; Murphy, E. J.; Basran, J.; Concilio, M. G.; Teixeira, S. C. M.; Schrader, T. E.; Fielding, A. J.; Ostermann, A.; Blakeley, M. P.; Raven, E. L.; Moody, P. C. E. *Science* **2014**, *345*, 193−197.
(71) Nonaka, D.; Wariishi, H.; Fujii, H. *Biochemistry* **2009**, *48*, 898−905.
(72) Nonaka, D.; Wariishi, H.; Welinder, K. G.; Fujii, H. *Biochemistry* **2010**, *49*, 49−57.
(73) A. Kimura, S.; Yamazaki, I. *Arch. Biochem. Biophys.* **1979**, *198*, 580−588.
(74) B. Maguire, R. J.; Dunford, H. B.; Morrison, M. *Can. J. Biochem.* **1971**, *49*, 1165−1171.
(75) Mukai, M.; Nagano, S.; Tanaka, M.; Ishimori, K.; Morishima, I.; Ogura, T.; Watanabe, Y.; Kitagawa, T. *J. Am. Chem. Soc.* **1997**, *119*, 1758−1766.

DOI: 10.1021/ja5107833
J. Am. Chem. Soc. 2015, 137, 349−361